THE ASTRONOMICAL JOURNAL VOLUME 106, NUMBER 2 AUGUST 1993

THE MASS–LUMINOSITY RELATION FOR STARS OF MASS 1.0 TO 0.08$\mathcal{M}_\odot$

TODD J. HENRY[1] AND DONALD W. MCCARTHY, JR.
Steward Observatory, Tucson, Arizona 85721
Electronic mail: thenry@stsci.edu, dmccarthy@as.arizona.edu

Received 1993 January 22; revised 1993 April 13

ABSTRACT

Mass–luminosity relations determined at infrared wavelengths are presented for stars with masses 1.0 to 0.08$\mathcal{M}_\odot$. Using infrared speckle imaging techniques on a sample of nearby binaries, we have been able to concentrate on the lower main sequence ($\mathcal{M} \leqslant 0.5\mathcal{M}_\odot$), for which an accurate mass–luminosity calibration has remained problematic. In addition, the mass–visual luminosity relation for stars with $2.0 \geqslant \mathcal{M} \geqslant 0.08\mathcal{M}_\odot$ is produced by implementing new photometric relations linking V to JHK wavelengths for the nearby stars, supplemented with eclipsing binary information. These relations predict that objects with masses $\sim 0.08\mathcal{M}_\odot$ have $M_K \sim 10$ and $M_V \sim 18$.

1. INTRODUCTION

Most stars are smaller, cooler, and intrinsically fainter than our Sun. In fact, a comparison of the Sun to the 100 nearest stars reveals that 88 are less massive, main-sequence dwarfs. Despite their dominance of the solar neighborhood, however, these objects remain poorly understood. For example, the fundamental dependence of intrinsic brightness upon mass—the mass–luminosity relation—remains ill-defined for low mass stars, and without an accurate calibration their contribution to the mass of the galaxy is a guess at best. In addition, the mass function that describes the low mass stellar population as a whole is impossible to determine correctly without an accurate mass–luminosity relation.

During our continuing survey of nearby stars for low mass companions (Henry & McCarthy 1990, 1992), it became obvious that an accurate, empirically-determined mass–luminosity relation (MLR) for the lowest mass stars was unavailable. For stars with masses $\leqslant 0.5\mathcal{M}_\odot$, Liebert & Probst (1987) presented the most comprehensive description of the MLR at the time in their Fig. 1, which compares $M_{\rm bol}$ and mass. Shown in that figure is the fit of Smith (1983), which was generated using points from Popper's (1980) review article on stellar masses. However, only seven stars in the Popper study had $\mathcal{M} \leqslant 0.3\mathcal{M}_\odot$, so the lowest mass stars were not well represented. Many of the additional low mass points included in the Liebert and Probst study were the result of preliminary infrared speckle work, which has led to the discovery of several very red, low mass secondaries orbiting stars in the solar neighborhood. As presented in 1987, their work provided a fundamental step forward from the status of well-determined M dwarf masses in 1980, but no attempt at a revised MLR was made. Two additional studies since then, Harmanec (1988) and Andersen (1991) have honed the MLR for stars more massive than the Sun (Andersen's Fig. 5 is the highest quality to date), but do not offer significant advances in the calibration of the MLR for lower mass stars.

In order to determine accurate masses and luminosities for a sample of low-mass stars, one is forced to use nearby binaries with high quality parallaxes. The best systems are those in which the components orbit at small separations so they have relatively short orbital periods, and permit confident orbit determinations. In addition to this rather severe restriction on the available pool of targets, calibrating the MLR for the reddest stars has been further compromised because of their weak flux in the visible, where the MLR is usually determined. By employing high resolution capability at infrared wavelengths, however, one can effectively study the close, red, low-mass binaries in detail. The ideal technique to be applied to this problem is infrared speckle imaging, which provides the high resolution necessary to split the close binaries ($\leqslant 2''$), and is carried out at infrared wavelengths where the targets are brightest.

Henry & McCarthy (1990) made the next step in defining the MLR for stars with masses $\leqslant 1.0\mathcal{M}_\odot$ using one-dimensional infrared speckle imaging. Continuing infrared speckle work, now expanded to two dimensions, combined with new parallaxes and improved orbits permits the calculation of more accurate masses and luminosities for the components of close doubles in the solar neighborhood. Furthermore, through the combination of infrared speckle imaging and long-term astrometric work, there are several resolved systems with very low-mass components, and the development of a strong relation, even at very low masses, is possible.

In this article, we present MLRs determined at near-infrared wavelengths, J (1.25 μm), H (1.6 μm) and K (2.2 μm), and provide updated masses for very red secondaries orbiting nearby stars. Earlier versions of the relations were reported in Henry & McCarthy (1990), but the relations are now far more robust, and the mass determinations more accurate. In addition, we define the mass–visual luminosity relation by implementing new infrared–visual photometric relations to estimate M_V values for constituents of the same binaries, supplemented with eclipsing binary data.

[1]Present address: The Space Telescope Science Institute, Baltimore, Maryland.

 0004-6256/93/106(2)/773/17/$0.90

Utilizing the MLRs detailed here we estimate absolute infrared and visible magnitudes for objects with masses 0.074 and 0.080$\mathcal{M}_\odot$, masses which span the transition region between stars and brown dwarfs of solar metallicity. These empirically-determined guidelines are especially useful because the most important parameter that would make a "brown dwarf candidate" a true brown dwarf—its mass—is extremely difficult to measure, while its intrinsic luminosity is comparatively easy to determine.

In the future, these MLRs will be used to characterize the numerically dominant population of the galaxy, the M dwarfs, including determinations of the ill-defined red dwarf mass function, and their contribution to the galactic mass.

2. SAMPLE AND OBSERVATIONS

2.1 Sample

The nearby stars provide an ideal venue for the calibration of the lower main sequence because high quality parallaxes are available, thereby leading to relatively small errors in absolute brightnesses and dynamically-determined masses. In addition, because of the low masses of the M dwarfs and their consequent slow orbital motion, only the closest systems will project measurable separations for binaries that have accurate visual or astrometric orbits determined.

A sample of close binaries with components of spectral types G2 and later was chosen to produce the infrared MLRs. The final sample includes 37 objects, listed in Table 1, all of which are members of binaries with main-sequence components, except for GL 166C, in which case component B is a white dwarf not used in the MLR derivations. The Worley & Heintz (1983) *Fourth Catalog of Orbits of Visual Binary Stars* was searched for systems with quality 1 orbits, considered to be definitive, in which the primary was of type G2 or later. Systems with quality 2 and 3 orbits with M dwarf primaries were then added in order to concentrate upon the reddest main-sequence stars. Finally, five astrometric binaries which have been resolved since the publication of the catalog by infrared speckle techniques have been added (see Sec. *3.1.2*). For the MLR at visible wavelengths, the visual/speckle binary sample has been combined with eclipsing binary data for components in 24 systems from Andersen (1991) and Popper (1980) to extend the MLR to 2.00$\mathcal{M}_\odot$.

2.2 Infrared Speckle Imaging and Photometric Observations

Observations of the close doubles have been made using both one-dimensional (1D) and two-dimensional (2D) infrared speckle imaging. Descriptions of the instrumentation and observing techniques can be found in McCarthy (1986) for 1D speckle, and McCarthy *et al.* (1990, 1991) for 2D speckle. Nearly all of the observations reported in Table 2 were made on the Steward Observatory 2.3 m telescope located on Kitt Peak, with a few observations from the KPNO 3.8 m also on Kitt Peak.

Infrared speckle observations provide the component separation, p, and the magnitude difference in the infrared (ΔJ,ΔH,ΔK). In the case of a set of 1D observations made at the same epoch (e.g., GL 623AB on 1986 Apr 20), and in all 2D observations, the position angle of the secondary, θ is also found, and can be used to check the accuracy of the binary system's astrometric orbit. The second column of Table 2 lists the wavelength of the speckle and photometric observations. The photometry for the *system* is given in column 3, except in the cases of GL 166C, 559AB and 725AB which are in wide binaries allowing individual photometry to be done on the components. The entry "relations" indicates that the components have M_V estimated using the relations discussed in Sec. *3.1.1*, so no apparent V photometry is required. Photometric references are given in column 4. An asterisk (*) indicates photometry provided by the authors using the 2D infrared speckle camera on the Steward Observatory 2.3 m telescope, or using the NICMOS 256×256 infrared camera provided by Marcia Rieke on the Steward Observatory 1.5 m telescope on Mt. Bigelow, Arizona. Photometric observations were made by taking multiple blocks of tens of frames on the target stars and Elias *et al.* (1982) standards of similar airmass. All data frames were then sky-subtracted, flat-fielded, and corrected for bad pixels. Errors include systematics determined by comparison of standard star data, and individual target errors found from the repeatability of a measurement at a given wavelength.

The fifth column gives the technique used for each speckle observation (1D or 2D). The scan direction is given in the case of 1D observations (e.g., NS=north–south, EW=east–west), and the camera field size for 2D observations (1X=8″, 2X=4″). The separations (in arcseconds), position angles, and magnitude differences are given in columns 7, 8, and 9. We have adopted a 10% error in separations obtained from the 1D data, which is representative of the uncertainty in the scanlength calibration and dominates any uncertainty in the fit to an individual dataset. The errors in the 2D data are determined from the individual errors in the fits for each dataset, and systematic errors caused by uncertainties in the separations and position angles of the binary star orbits used for plate-scale determination (±4% in separation) and orientation on the sky (±2°). In the case of multiple observations at the same wavelength, the adopted Δm has been found by a weighted mean of the individual measurements and is given in a separate line.

The filters used in the 1D observations included the infrared J ($\lambda\lambda$=1.11–1.38 μm, λ_0=1.24 μm), H ($\lambda\lambda$=1.35–1.87 μm, λ_0=1.62 μm), and K ($\lambda\lambda$=1.77–2.48 μm, λ_0=2.17 μm) bands. The filters in the 2D camera were of slightly different passband: J ($\lambda\lambda$=1.07–1.39 μm, λ_0=1.24 μm), H ($\lambda\lambda$=1.44–1.82 μm, λ_0=1.62 μm), and K ($\lambda\lambda$=1.96–2.43 μm, λ_0=2.19 μm). No adjustments have been made between the two filter sets because typically the errors in the final absolute magnitudes used in the MLRs are dominated by errors in the measured magnitude differences and parallaxes.

TABLE 1. Basic information and orbital parameters for nearby binaries.

GL #	Other	RA (1950.0)	DEC (1950.0)	$\pi\pm\sigma$	P (yrs)	a (″)	B	q	References
22AC†	BD +66°34	00 29 20	+66 57 48	.1006 .0022	15.95	0.498	0.261	ast	Hr 73, MHMC 91, *
					0.22	0.012	0.005		
25AB	HD 3443	00 34 47	−25 02 30	.0721 .0087	25.00	0.670	0.5	1	V 37, S 63
					0.13	*0.007*	*0.02*		
65AB	L726-8	01 36 25	−18 12 42	.3807 .0043	26.52	1.95	0.494	(2)	GHW 88
					0.40	*0.059*	0.003		
67AB†	HD 10307	01 38 44	+42 21 48	.0731 .0039	19.50	0.565	0.231	ast	LBM 83, HMFC 92, *
					0.28	0.035	0.014		
166BC	HD 26976	04 13 04	−07 44 06	.2071 .0025	252.1	6.943	0.262	3	Hz 74
					6.30	*0.347*	0.01		
234AB†	Ross 614	06 26 51	−02 46 12	.2421 .0017	16.60	1.009	0.317	ast	P 77, JHM 93, *
					0.03	0.087	0.025		
340AB	HD 79969	09 14 56	+28 46 42	.0582 .0029	34.20	0.66	0.473	(1)	V 38, Hr 82
					0.17	*0.007*	0.006		
352AB	BD −12°2918	09 28 53	−13 16 06	.1079 .0091	18.3	0.551	0.51	3	Hz 79
					0.46	0.03	*0.02*		
508AB	HD 115953	13 17 36	+48 02 24	.1030 .0080	48.85	1.465	0.412	2	Hz 69, Hz 76
					0.73	*0.044*	0.012		
559AB	α Cen	14 36 11	−60 37 48	.7506 .0046[a]	79.92	17.515	0.454	(1)	KW 78, Hz 82, DGV 86
					0.40	0.05	0.002		
570BC[b]	HD 131976	14 54 31	−21 11 18	.1742 .0060	0.848	0.143	0.414	sp	MPDD 90
					0.001	0.009	*0.01*		
623AB†	G 202-45	16 22 39	+48 28 24	.1317 .0039	3.73	0.271	0.183	ast	LB 78, MH 87, MM 89, *
					0.09	0.031	0.020		
661AB	HD 155876	17 10 40	+45 44 48	.1595 .0031	12.98	0.71	0.496	(1)	E 67, HzB 84
					0.03	0.01	0.01		
677AB	BD +29°3029	17 27 24	+29 26 00	.0482 .0045	60.00	0.60	0.468	3	B 55, L 82
					1.50	*0.030*	0.011		
702AB	HD 165341	18 02 56	+02 30 36	.1990 .0036	88.13	4.545	0.442	(1)	WH 74
					0.44	*0.045*	0.01		
704AB	HD 165908	18 05 08	+30 33 12	.0592 .0039	55.8	1.00	0.398	1	Hz 72
					0.28	*0.010*	0.01		
725AB	HD 173739/40	18 42 12	+59 33 18	.2861 .0018	408	13.88	0.46	(3)	Hz 87
					10.2	*0.694*	0.02		
1245AC†	G 208-44	19 52 16	+44 17 30	.2206 .0014[c]	15.22	0.795	0.365	ast	MHFSLC 88, Ha 90, *
					0.08	0.043	0.019		
860AB	HD 239960	22 26 13	+57 26 48	.2519 .0023	44.67	2.383	0.394	(1)	Hz 86b
					0.22	*0.024*	0.002		

Notes to TABLE 1

[a] parallax from Demarque *et al.* (1986)

[b] see Mariotti *et al.* (1990) for mass solution from spectroscopic and speckle data, note that the parallax listed (from Gliese and Jahreiss 1991) will not yield the masses given in Table 5

[c] parallax from Harrington (1990)

† semimajor axis and fractional mass determined via speckle data and photometric relations

Italicized quantities indicate errors estimated by the authors.

References for TABLE 1

B 55 = Baize (1955), E 67 = Eggen (1967), DGV 86 = Demarque *et al.* (1986),
GHW 88 = Geyer *et al.* (1988), Ha 90 = Harrington (1990), Hr 73, 82 = Hershey (1973, 1982),
Hz 69, 72, 74, 76, 79, 82, 86b, 87 = Heintz (various years), HzB 84 = Heintz and Borgman (1984),
HMFC 92 = Henry *et al.* (1992), JHM 93 = Johnson *et al.* (1993), KW 78 = Kamper and Wesselink (1978),
L 82 = Lippincott (1982), LB 78 = Lippincott and Borgman (1978); LBM 83 = Lippincott *et al.* (1983),
MHFSLC 88 = McCarthy *et al.* (1988), MH 87 = McCarthy and Henry (1987), MHMC 91 = McCarthy *et al.* (1991),
MM 89 = Marcy and Moore (1989), MPDD 90 = Mariotti *et al.* (1990), P 77 = Probst (1977),
S 63 = Strand (1963), V 37 = van den Bos (1937), V 38 = van den Bos (1938),
WH 74 = Worth and Heintz (1974), * = this work

1993AJ....106..773H

TABLE 2. Photometric and infrared speckle observations.

GL #	λ	Phot	Ref	Tech	Date	Separation	PA	Δm ± σ
22AC	H	6.58 0.08	MHMC	2D 2X	10 Dec 89	0.453 0.020	044 03	2.11 0.06
	K	6.26 0.09	MHMC	2D 2X	12 Oct 89	0.451 0.020	043 03	1.94 0.06
	V	relations						
25AB	H	3.96 0.03	*	2D 2X	11 Dec 89	0.687 0.026	110 02	0.25 0.02
	K	3.85 0.07	*	2D 2X	11 Dec 89	0.687 0.026	110 02	0.16 0.01
65AB	J			1D EW	09 Nov 87	0.63 0.06	E	0.62 0.07
	J			2D 1X	29 Nov 90	2.135 0.082	005 02	0.33 0.03
	J	6.24 0.03	L				adopt	0.38 0.03
	H	5.67 0.03	L	1D NS	08 Nov 87	2.11 0.21	N	0.30 0.02
	K	5.33 0.03	L	1D EW	07 Feb 88	0.70 0.07	E	0.40 0.07
	V	relations						
67AB	J	3.80 0.04	HMFC	2D 2X	01 Dec 90	0.448 0.030	194 02	4.37 0.25
	H	3.56 0.04	HMFC	2D 2X	28 Nov 90	0.442 0.018	199 02	4.50 0.12
	K			2D 2X	10 Oct 89	0.623 0.027	203 02	4.30 0.07
	K			2D 2X	07 Dec 90	0.485 0.025	196 02	4.50 0.05
	K	3.53 0.04	HMFC				adopt	4.43 0.04
	VA	4.96 0.05	JMM					
	VB	relations						
166C	J	6.91 0.07	*					
	H	6.29 0.07	*					
	K	6.00 0.07	*					
	V	11.19 0.05	L					
234AB	see Johnson *et al.* 1993 for observations							
	J	6.38 0.03	L				adopt	1.79 0.30
	H	5.78 0.03	L				adopt	1.63 0.11
	K	5.49 0.03	L				adopt	1.50 0.10
	V	relations						
340AB	J	5.31 0.04	*	2D 2X	27 Apr 91	0.153 0.006	295 02	0.35 0.01
	H	4.84 0.04	*	2D 2X	11 Dec 89	0.203 0.010	256 02	0.42 0.01
	K	4.71 0.04	*	2D 2X	11 Dec 89	0.203 0.008	256 02	0.08 0.08
352AB	J	6.36 0.03	L	1D NS	22 Jan 89	0.48 0.05	N	0.33 0.05
	H	5.79 0.03	L	1D NS	22 Jan 89	0.47 0.05	N	0.26 0.02
	K	5.57 0.03	L	1D NS	22 Jan 89	0.48 0.05	N	0.23 0.02
	V	relations						
508AB	J	5.31 0.03	SH	1D EW	18 Feb 89	0.97 0.10	W	1.08 0.07
	H	4.69 0.03	SH	1D EW	18 Feb 89	0.98 0.10	W	0.98 0.02
	K	4.50 0.03	SH	1D EW	18 Feb 89	0.98 0.10	W	0.92 0.02
	V	relations						
559A	J	−1.14 0.05	ESWS					
	H	−1.38 0.05	ESWS					
	K	−1.48 0.05	ESWS					
	V	0.33 0.05	ESWS					
559B	J	−0.01 0.05	ESWS					
	H	−0.49 0.05	ESWS					
	K	−0.60 0.05	ESWS					
	V	1.70 0.05	ESWS					
570BC	see Mariotti *et al.* 1990 — adopted Δm values from combined data							
	J			2D 2X	11 Feb 90	0.153 0.006	220 02	1.30 0.04
	J	4.75 0.03	L				adopt	1.30 0.04
	H	4.14 0.03	L				adopt	1.19 0.12
	K	3.93 0.03	L				adopt	1.12 0.07
	V	relations						
623AB	J	6.67 0.03	L	1D NS	14 Mar 87	———	———	3.28 0.3
	H			1D NS	14 Mar 87	0.26 0.03	———	3.00 0.3
	H			2D 2X	27 Apr 91	0.190 0.008	338 02	2.65 0.03
	H	6.14 0.03	L				adopt	2.65 0.03
	K			1D NS	07 May 82	0.28 0.03	———	3.04 0.32
	K			1D EW	09 Jul 82	0.25 0.03	———	———
	K			1D NESW[a]	20 Apr 86	0.39 0.04	NE	2.85 0.26
	K			1D NS[a]	20 Apr 86	0.28 0.04	N	———
	K			1D NESW	18 Jun 86	0.33 0.03	NE	2.81 0.23
	K			1D NS	10 Jan 87	0.35 0.04	N	2.85 0.31
	K	5.91 0.03	L				adopt	2.87 0.14
	V	relations						

1993AJ....106..773H

TABLE 2. (continued)

GL #	λ	Phot	Ref	Tech	Date	Separation	PA	Δm ± σ	GL #	λ	Phot	Ref	Tech	Date	Separation	PA	Δm ± σ
661AB	J	5.56 0.03	L	1D NS	20 Mar 89	0.68 0.07	S	0.41 0.01	725A	J	5.20 0.03	L					
	H	5.04 0.03	L	1D NS	20 Mar 89	0.70 0.07	S	0.46 0.02		H	4.67 0.03	L					
	K	4.82 0.03	L	1D NS	20 Mar 89	0.70 0.07	S	0.42 0.07		K	4.44 0.03	L					
	V	relations								V	8.90 0.05	L					
677AB	J	6.62 0.04	*	1D EW	21 Jun 89	0.73 0.07	W	0.30 0.02	725B	J	5.72 0.03	L					
	H	6.08 0.03	*	1D EW	21 Jun 89	0.74 0.07	W	0.31 0.03		H	5.20 0.03	L					
	K	5.90 0.09	*	1D EW	21 Jun 89	0.72 0.07	W	0.28 0.03		K	4.97 0.03	L					
	V	relations								V	9.68 0.05	L					
702AB	J	2.41 0.05	*	2D 1X	20 Aug 91	1.571 0.060	205 02	1.51 0.04	1245AC	J			1D EW[b]	08 Jun 87	0.89 0.09	E	1.22 0.04
	H	———		2D 2X	11 Oct 89	1.484 0.057	233 02	———		J			1D EW	06 Sep 87	0.86 0.09	E	1.34 0.04
	K			2D 2X	11 Oct 89	1.475 0.057	233 02	———		J			1D EW[c]	06 Oct 87	1.00 0.10	E	1.12 0.07
	K			1D NS	24 Oct 83	1.09 0.11	———	0.77 0.07		J	7.78 0.03	L				adopt	1.26 0.03
	K			1D NS	26 Sep 83	1.03 0.10	———	0.74 0.05		H			1D EW	18 Sep 86	0.81 0.08	E	1.15 0.04
	K			1D EW	25 Sep 83	1.85 0.19	———	0.72 0.05		H			1D EW[b]	08 Jun 87	0.90 0.09	E	1.07 0.02
	K	1.96 0.03	P				adopt	0.74 0.03		H			1D EW[c]	06 Oct 87	1.00 0.10	E	1.04 0.07
	VA	4.21 0.05	GJ							H	7.26 0.03	L				adopt	1.08 0.02
	VB	6.00 0.05	GJ							K			1D NS	09 Nov 84	0.39 0.04	———	1.19 0.09
										K			1D EW[b]	08 Jun 87	0.90 0.09	E	1.02 0.02
704AB	J	3.66 0.07	*	2D 1X	28 Apr 91	0.971 0.037	027 02	2.53 0.02		K	6.89 0.03	L				adopt	1.03 0.02
	H	3.50 0.04	*	2D 2X	10 Feb 90	1.048 0.040	024 02	2.40 0.07		V	relations						
	K	3.37 0.10	*	1D NS	21 Mar 89	1.00 0.10	N	2.06 0.07									
	VA	5.09 0.05	GJ						860AB	J	5.56 0.03	L	1D NS	07 Jul 88	2.45 0.25	S	1.19 0.10
	VB	8.45 0.05	GJ							H	4.97 0.03	L	1D NS	07 Jul 88	2.46 0.25	S	1.14 0.05
										K	4.71 0.03	L	1D NS	07 Jul 88	2.41 0.24	S	1.37 0.08
										V	relations						

Notes to TABLE 2

[a] for mass determinations, combined 1D observations yield 0.39″ at 44°
[b] for mass determinations, combined 1D observations yield 0.90″ to the east
[c] for mass determinations, combined 1D observations yield 1.00″ to the east

References for TABLE 2

ESWS = Engels *et al.* (1981),
GJ = Gliese and Jahreiss (1991),
HMFC = Henry *et al.* (1992),
JMM = Johnson *et al.* (1968),
L = Leggett (1992),
MHMC = McCarthy *et al.* (1991),
P = Probst (1981) Table A.7,
SH = Stauffer and Hartmann (1986),
* = this work

3. DATA

3.1 Masses

3.1.1 Mass derivation parameters: New infrared–visible photometric relations

In order to determine the dynamical masses of the components in a binary, four parameters must be known: period, semimajor axis of the relative orbit, fractional mass, and parallax. In the cases of the visual binaries in the current sample, all of these parameters are known and mass determinations are straightforward through Kepler's Third Law. For astrometric binaries, the period and parallax are known, and once the system is resolved using infrared speckle imaging, the semimajor axis and fractional mass can be determined as follows.

The semimajor axis, a, is found from the semimajor axis of the photocentric orbit, α, multiplied by the scale factor of the relative to astrometric orbits. This is possible because the relative orbit has properties identical to the astrometric orbit (P, T, e, i, ω, and $\Omega+180°$ [phase shift required because the relative orbit measures the position angle of the secondary with respect to the primary, whereas the photocentric orbit describes the perturbation of the center of light, dominated by the primary]), except for the size which is described by the semimajor axis.

The scale factor is found from speckle observations at one or more epochs, where the faint companion is found at a separation p. This observed separation is divided by the predicted photocentric perturbation at that epoch, ρ, to obtain a measurement of the scale factor, and the average scale factor is then found from a series of speckle observations.

The errors in the scale factors for the five astrometric binaries discussed here have been found from the standard deviation of several infrared speckle observations. In three cases, the companions have only recently been imaged for the first time, and errors in the scale factors should be considered preliminary: GL 22AC (observations spanning only 2 months, error in scale factor, 1%), GL 67AB (14 months, error 6%), and GJ 1245AC (35 months, error 5%). Only continual monitoring of the orbits will allow more accurate determinations of the errors. For the remaining two systems, more than a complete orbit is covered by speckle data, and the scale factor errors are well-determined: GL 234AB (2.2 orbits, error in scale factor 8%) and GL 623AB (2.4 orbits, error 11%).

The final parameter to be determined, the fractional mass of the secondary, $B=\mathcal{M}_B/(\mathcal{M}_A+\mathcal{M}_B)$, can be found for an astrometric binary using $B=(\rho/p)+\beta$, in which β is the fractional distance of the primary to the photocenter in terms of the separation of the binary. Because the secondaries have not been seen in the visible, β must be estimated from the infrared data. Two steps are required. First, the conversion of an infrared magnitude difference to a visual magnitude difference, ΔV, is accomplished using the new absolute infrared magnitude–color relations discussed here. Then, β is found from ΔV using the calibration of Feierman (1971).

In the past, the brightness difference in the visible was estimated by converting from the observed difference in the infrared to ΔV using the relations for low mass binaries found by Probst (1981): $\Delta J/\Delta V=0.56$, $\Delta H/\Delta V=0.55$, $\Delta K/\Delta V=0.53$. These relations, however, do not consider the second-order color effects which are important for very red secondaries. For example, consider two binaries with $\Delta K\sim 1.6$, where the components have been moved to the same distance and combined into hypothetical systems. $\Delta K=1.61$ for the dM0.0/dM3.0 pair GL 338A/GL 725A, and is nearly identical ($\Delta K=1.62$) to the dM4.5/dM8.0 pair GL 83.1/GL 752B (VB 10). However, because of the extreme redness of VB 10, the ΔV for the latter pair is much larger ($\Delta V=4.70$) than for the former ($\Delta V=2.51$), although the Probst relations would predict the same value.

In order to estimate more accurately the brightness difference in the visible, we have developed absolute magnitude–color relations using only those stars that are "single" according to current data (see Table 3). The quotes have been used here because for the present purposes, we only require a star's photometry to be representative of a single body, unaffected by any close (less than 10 AU), relatively bright companion. We cannot rule out the presence of very low luminosity, substellar companions that remain undetected, but such objects will contribute very little to the visible or infrared flux of the system, and will therefore not significantly affect the relations discussed below. Companions orbiting at greater than 10 AU that are bright enough to affect the photometry would have been detected visually. Wide systems for which accurate photometry can be acquired for each component remain in the list.

TABLE 3. "Single" red dwarfs used in photometric relations.

15A	K,MB,T	393	MB	699	K,MB	solid points
15B	K,MB	402		701	MB	
54.1		406		725A	K,T	GL 752B
83.1		408		725B	K,T	LHS 191
105B		411	K,MB	729		LHS 523
109	MB	412A	MB	752A	MB	LHS 2397a
166C*	K	412B*		809	T	LHS 2471
169.1A		445		873	MB	LHS 2930
205	MB	447	K,MB	880	MB,T	LHS 3003
213	MB	450		884		
229	MB	514		905		starred points
251	MB	526	K,MB	908	MB,T	
273	K,MB	555		1002*		LHS 2065
299*		581	MB	1111		LHS 2924
300*		625		1156*		
338A	MG	628	K	1245B		
338B	MG	643		LHS 292*		
388	MB	644C*				

Notes to TABLE 3

* searched 2 to 10 AU with infrared speckle; all others in first three columns were searched 1 to 10 AU

References for TABLE 3

K = Kenyon (1993)
MB = Marcy and Benitz (1989)
MG = Morbey and Griffin (1987)
T = Tokovinin (1992)

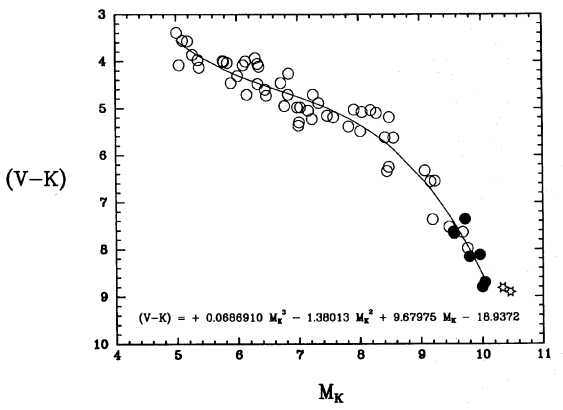

FIG. 1. $(V-K)$ vs M_K relation for red dwarfs. Points include stars known to be "single" (open points), very red, presumed single dwarfs (solid points), and the very low-mass objects LHS 2065 and LHS 2924 (starred points).

For the 53 objects listed by Gliese number in the first three columns of Table 3, no companions were found orbiting between 1 and 10 AU (2 and 10 AU in 8 cases, indicated by *) during our infrared speckle survey of all northern M dwarfs within 8 parsecs (Henry & McCarthy, 1990, 1992). In addition, 28 of these stars have sufficient radial velocity coverage to rule out stellar companions within 1 AU not resolved by speckle work, as discussed in the appropriate velocity references: Kenyon (1993), Marcy & Benitz (1989), Morbey & Griffin (1987), and Tokovinin (1992). Many of the 25 remaining stars are included in the continuing CORAVEL and CfA radial velocity surveys, but at the present time there is no published evidence that they possess stellar companions.

The 53 "single" stars with *VJHK* photometry (open points) have been fit with fourth-order polynomials to relate absolute infrared magnitudes to color, as illustrated for K in Fig. 1. A significant improvement in rms was made in moving from third- to fourth-order fits (for example, 14% in the K fit), but higher order fits did not result in significant decreases in the rms and therefore have not been used (at K, the fifth-order fit rms was only 1.2% better than the fourth-order fit). In order to bolster the red end of the calibration, seven additional stars of very late type (solid points) that we *assume* are single have been added: GL 752B, LHS 191, 523, 2397a, 2471, 2930, and 3003.

The functional forms of the fits are described by

$$(V-K)=0.0686910M_K^3-1.38013M_K^2+9.67975M_K-18.9372$$
$$\text{rms in}(V-K)=0.30 \text{ mag}, \quad (1a)$$

$$(V-H)=0.0527610M_H^3-1.08854M_H^2+7.90535M_H-15.6925$$
$$\text{rms in}(V-H)=0.28 \text{ mag}, \quad (1b)$$

$$(V-J)=0.0416816M_J^3-0.928176M_J^2+7.38930M_J-17.0052$$
$$\text{rms in}(V-J)=0.25 \text{ mag}. \quad (1c)$$

We list the rms values for the fits, rather than the standard deviations, because the scatter in the points is due to true differences between stars of a given luminosity or color, not to errors in the measurements. The various ages and metallicities of objects included in the sample cause the scatter to be much larger than errors in the absolute magnitudes or colors, both typically 0.06 to 0.08 mag.

A detailed discussion of the effects of age and metallicity on low mass star color–luminosity relations can be found in Leggett (1992). Of the 60 stars used to develop the relations above, 53 have kinematic and/or photometric population information given by Leggett, heavily weighted to the old disk population. Only three stars appear to be part of the halo population, so we will concentrate on differences between the young and old disk populations only. From her Fig. 14 and Table 5, for example, it is apparent that for $(V-K)=4.0$, M_K values range from 5.3 at young-disk age to 6.0 at old-disk age. At $(V-K)=6.0$, the corresponding M_K values are 8.1 and 8.4. For redder $(V-K)$, the difference is smaller, though the relation in this regime is not well calibrated. This limits the accuracy with which it is possible to estimate a color or luminosity for an individual star given the complementary parameter. We emphasize that the relations presented here allow us to predict an *average* color for a star in the solar neighborhood based upon knowledge of a star's luminosity in one of the infrared bands, and the rms values given provide an estimate of the accuracy one can expect in the color or luminosity for an individual star. Complementary fourth-order fits, e.g., M_K vs $(V-K)$, result in rms values of 0.41 mag at M_K, 0.42 at M_H, and 0.35 at M_J.

The fits provided here are valid for objects with $5.0 \leqslant M_K \leqslant 10.0$, $5.1 \leqslant M_H \leqslant 10.5$, and $5.7 \leqslant M_J \leqslant 11.2$. Much of the photometry has been taken from the Leggett work and has been supplemented by this group. Parallaxes for the fitted points are from the *Third Catalog of Nearby Stars* by Gliese & Jahreiss (1991). The full set of photometric data will be given in a future paper.

The two starred points plotted in Fig. 1 represent the very faint, very red objects LHS 2924 and LHS 2065. These two objects do not follow the trend of the other points and have not been included in the fit. Probst & Liebert (1983) discuss the anomalous colors of LHS 2924 in detail, including a V excess of ~ 1 mag relative to M dwarfs of earlier type (M7 and M8), causing it to appear blue in Fig. 1. Spectral anomalies include saturated TiO bands and prominent VO features. It is possible that these two objects are high-mass brown dwarfs, and not true stars at all (see Sec. *5.2*).

Using these three relations, we can estimate V for the members of close binaries because the system infrared photometry, infrared brightness difference and parallax yield J, H, K, M_J, M_H, and M_K for each component. We obtain three sets of V magnitudes that yield three estimates of ΔV.

TABLE 4. Test cases for new photometric relations.

GL #	Sep.	Method	ΔV(J)	ΔV(H)	ΔV(K)	ΔV Result
15AB	32″	Probst	3.48	3.60	3.66	3.58 ± 0.09
		this paper	3.12	3.05	3.06	3.08 ± 0.04
		actual				2.99
338AB	17″	Probst	0.13	0.11	0.15	0.13 ± 0.02
		this paper	0.12	0.11	0.16	0.13 ± 0.03
		actual				0.09
412AB	28″	Probst	5.55	5.76	5.83	5.71 ± 0.15
		this paper	5.42	5.48	5.56	5.49 ± 0.07
		actual				5.64
725AB	13″	Probst	0.93	0.96	1.00	0.96 ± 0.04
		this paper	0.79	0.77	0.77	0.78 ± 0.01
		actual				0.78
752AB	74″	Probst	7.86	7.93	7.81	7.87 ± 0.06
		this paper	8.75	8.68	8.55	8.66 ± 0.10
		actual				8.38

These are then averaged to determine ΔV and its error for the system. Five nearby late-type binaries of relatively wide separation have been tested to confirm that this new method is more accurate than the Probst relations, and details are given in Table 4. Significant improvement can be seen in the ΔV values for GL 15AB, 725AB, and 752AB (ΔV from Probst differs from the actual values by 0.59, 0.18, and 0.51 mag, respectively, compared to 0.09, 0.00, and 0.28 mag using the new relations), although for 412AB the estimate is slightly worse (0.07 for Probst, 0.15 here). We conclude that the method used here is superior to the Probst relations in most cases. An additional check on the accuracy of ΔV can be made using the area scanner work of Rakos *et al.* (1982). The only pair common to that sample and this one for which ΔV was estimated via the new relations is GL 65AB; we find $\Delta V=0.87$ and they measure $\Delta V=0.84$.

Once ΔV has been determined, the calibration of Feierman (1971) yields the desired quantity β from ΔV. Feierman found that care must be taken in the estimation of β for close astrometric binaries with a magnitude difference in the visible greater than 1.0 mag. However, in the case of the five astrometric binaries discussed here, ΔV is so large that only a very small amount of the light at V is contributed by the secondary, resulting in very small (or zero) values for β. In fact, the β term accounts for less than 5% of the fractional mass values for the resolved astrometric binaries listed in Table 1: GL 22AC ($\beta=0.010\pm0.004$), GL 67AB ($\beta=0$), GL 234AB ($\beta=0.009\pm0.005$), GL 623AB ($\beta=0$), and GJ 1245AC ($\beta=0.012\pm0.003$). Thus, the reservations expressed by Feierman, while warranted, do not affect significantly the determination of the fractional mass of the secondary for the binaries discussed here, for which errors in the ratio ρ/p dominate uncertainties in B.

Finally, the fractional mass of the secondary can be found from $B=(\rho/p)+\beta$. The set of parameters required to compute the dynamical masses for an astrometric binary is then complete, using the combination of astrometric and speckle data.

3.1.2 Masses determined using infrared speckle imaging

Here we discuss five astrometric systems for which infrared speckle resolution has allowed the determination of the component masses: GL 22AC, 67AB, 234AB, 623AB, and GJ 1245AC. These systems include five of the seven least luminous objects for which reliable masses have been determined, all with $\mathcal{M}<0.15\mathcal{M}_\odot$. The masses given here supercede those in the references listed, due to additional recent observations, implementation of the better method to estimate the fractional masses discussed in the previous section, and the availability of new parallaxes from Gliese & Jahreiss (1991). In the following discussion, BR designates brightness ratio.

GL 22AC (McCarthy *et al.* 1991): Using the two infrared speckle measurements reported we now estimate $\Delta V=3.26\pm0.15$ using the relations described above, rather than 3.66. This change results in a fractional mass, $B=0.261\pm0.005$, and with the new parallax of 0.1006 ±0.0022 we find masses of 0.352 ± 0.036 and $0.124\pm0.013\mathcal{M}_\odot$, less than a 3% change from the previous values.

GL 67AB (Henry *et al.* 1992): The large flux ratio in the infrared, $BR=60$–70, leads to $\beta=0$ and B remains unchanged. Using the relations above and the new parallax of 0.0731 ± 0.0039, we can now accurately estimate the absolute visual magnitude of the secondary ($M_V=11.8$) and compute the brightness ratio in the visible: $\Delta V=7.5$, or $BR\approx1000$. Due to the new parallax for the system, a 4% revision is masses is required, yielding component masses of 0.933 ± 0.231 and $0.280\pm0.071\mathcal{M}_\odot$.

GL 234AB (Probst 1977; Johnson *et al.* 1993): This is the well-studied, nearby double, Ross 614AB. We now have observations of the pair in the infrared at seven different epochs from 1985 to 1992. These seven observations have been combined with five visual observations given in Probst (1977), one visible speckle point listed in McAlister & Hartkopf (1988), the updated parallax of 0.2421 ±0.0017, and our new fractional mass determination, $B=0.317\pm0.025$ ($\Delta V=3.33\pm0.26$), to obtain masses of 0.179 ± 0.047 and $0.083\pm0.023\mathcal{M}_\odot$. With such a low mass, GL 234B should be considered a viable brown dwarf candidate. A full discussion of the system will be given in Johnson *et al.* (1993).

GL 623AB (McCarthy & Henry 1987; Marcy & Moore 1989): As indicated in both the infrared speckle and radial velocity studies, the primary appears overmassive for its brightness. This has been proposed to be due to either a poorly determined parallax or an incorrect semimajor axis determination from the speckle work. We now have an additional speckle point using the 2D camera, which can be used to fix the ascending node by requiring the astrometric orbit to match the observed speckle position angle. We find $\Omega=121°$, and a comparison using the only other observational epoch when the position angle can be determined (1D speckle observations at 0° and 45° on 1986.299) indicates a small $(O-C)$ in position angle: $44°-41°=3°$.

The $(O-C)$ values at these two epochs [1986.299, 1991.321], [0°,+3°], are significantly better than those found using the Ω value of McCarthy and Henry [+15°, +12°], or that of Marcy & Moore [−18°, −21°].

Adopting the full set of orbital elements for the system, $P=3.73$ y, $T=1984.45$, $e=0.566$, $i=147.3°$, $\omega=262°$ and $\Omega=121°$, and including the best five speckle observations to find the semimajor axis, $a=0.271\pm0.031$, and $B=0.183\pm0.020$ ($\Delta V=5.50\pm0.79$), we find masses of 0.511 ± 0.182 and $0.114\pm0.042\mathcal{M}_\odot$, which are similar to those reported by McCarthy and Henry. Marcy and Moore derived independent measures of the secondary's mass using an adopted mass for the primary of $0.34\pm0.04\mathcal{M}_\odot$, assigned by photometric techniques. They find $\mathcal{M}_B=0.080\pm0.030$ using their radial velocity data, and $\mathcal{M}_B=0.081\pm0.014$ from the astrometry and the adopted primary mass. However, as is discussed in Sec. *4.1*, photometric mass estimates for red dwarfs between 0.50 and $0.18\mathcal{M}_\odot$ are uncertain, and these low secondary mass estimates that are based upon an assumed primary mass must be considered tentative. While the lower masses may in fact be closer to the true masses, we are forced to adopt the higher values, obtained without any reliance upon a photometric calibration for the primary, until further data are acquired to measure the relative orbit more accurately.

GJ 1245AC (McCarthy *et al.* 1988; Harrington 1990): This low mass triple, in which the brighter visual component has a very low-mass companion ($\Delta V=3.18\pm0.13$), has the best determined masses of any of the very low mass objects. We have rederived the masses using the original 1D speckle data, the new orbit provided by Harrington which is considered definitive, his parallax of 0.2206 ± 0.0014, and the new fractional mass technique, which yields $B=0.365\pm0.019$. The final masses are 0.128 ± 0.021 and $0.074\pm0.013\mathcal{M}_\odot$, placing GJ 1245C in the realm of brown dwarf candidates.

3.1.3 Masses used in relations

Table 1 shows the orbital parameters and the references used in determining the masses and errors of the 37 stars used in the MLRs. Column 5 lists the adopted parallax and its standard error for each system. Most parallaxes have been taken from the *Third Catalog of Nearby Stars* by Gliese & Jahreiss (1991). The next three columns list the orbital parameters required to determine component masses—the period (P), semimajor axis (a), and fractional mass (B), and their errors. Column 9 lists the quality of the orbit, as given in Worley & Heintz (1983), or as "ast" in the case of astrometric orbits. The "sp" listed for GL 570BC indicates that the orbit is a speckle/spectroscopic one, rather than visual or astrometric. In cases where recent orbits have been used, we have estimated the orbit qualities (given in parentheses) following the Worley and Heintz guidelines. In most cases, the new orbits are slight revisions of quality one orbits. The orbit references are included in the final column.

Standard errors for the period and semimajor axis were estimated when they were not given in the original papers, and are shown in the table italicized. One percent errors in a, and one-half percent in P were adopted for well-observed binaries with quality 1 "definitive" orbits. In all cases, the orbital motion of these binaries has been followed for more than one full revolution with consistent coverage throughout. The periods are generally better determined than the semimajor axes, hence the smaller proportional error. Three percent errors were adopted in a and 1.5% in P for those systems with quality 2 orbits. Five percent in a and 2.5% in P were assumed for the quality 3 orbits of GL 166BC, 677AB and 725AB, which have been followed for less than a full revolution, and for GL 352AB which has limited observations. The magnitudes of these estimated errors are similar to the errors reported by authors for various systems in which the errors are given (c.f. Eggen 1967), although they are larger than errors adopted by Popper (1980). In several cases (e.g., GL 677AB, 702AB) the mass errors computed here from the full analysis are similar to errors given for the masses in the original paper, although in the case of GL 166C this is not true. In this instance, we have adopted a larger mass error ($0.026\mathcal{M}_\odot$) than reported by Heintz (1974, probable error $0.01\ \mathcal{M}_\odot$) which would require errors of 1% in P and 2% in a. These small errors appear unlikely, considering that only 122 years of the 252 year orbit have been followed, except for two critical points before 1851.

The derived component masses are given in column 2 of Table 5, with their formal 1σ errors. The errors include standard and estimated errors in the parallax, the period, the semimajor axis, and the fractional mass. We note that because the errors on the semimajor axis enter into Kepler's Law as the cube, the final masses are critically sensitive to both the axis measured and the parallax.

3.1.4 Systems with very low mass components not used in relations

Here we discuss six systems which contain very low mass objects, but which have not been used to determine the MLRs because it is premature to include them without better data.

GJ 1005AB (Ianna *et al.* 1988; Heintz 1990): Also known as LHS 1047AB, accurate mass calculations have proven problematic because of the small separation of the pair (never measured more than 0.4"), resulting in astrometric solutions with large errors in the semimajor axis and fractional masses. There are currently two strong 1D and one 2D infrared speckle measurements by our group, and three visible micrometer measurements by Heintz. The Heintz orbit ($P=4.88$ years, $\alpha=0.100''$) fits the infrared observations somewhat better than the Ianna *et al.* orbit ($P=4.63$ years, $\alpha=0.073''$), although when either is used, the formal errors in the masses are larger than the masses themselves. Obviously, further work is needed. The secondary probably contains roughly a third of the system mass, and is likely to have a mass near or below $0.08\mathcal{M}_\odot$, making it an important target for future speckle work. It is encouraging that further speckle observations will result in accurate masses, since the parallax and period are relatively well determined.

GL 473AB (Heintz 1989; Henry *et al.* 1992): Speckle observations indicate that the secondary is not following

TABLE 5. Derived quantities: Absolute magnitudes and masses.

GL #	Mass ± σ	$M_V \pm \sigma$	$M_J \pm \sigma$	$M_H \pm \sigma$	$M_K \pm \sigma$
22A	0.352 0.036	10.99 0.06	—	6.74 0.08	6.44 0.10
22C	0.124 0.013	14.25 0.20	—	8.85 0.10	8.38 0.11
25A	0.642 0.235	—	—	3.88 0.26	3.82 0.27
25B	0.642 0.235	—	—	4.13 0.26	3.98 0.27
65A	0.097 0.010	15.09 0.10	9.72 0.04	9.19 0.04	8.80 0.05
65B	0.094 0.010	15.95 0.07	10.10 0.04	9.49 0.04	9.20 0.06
67A	0.933 0.231	4.28 0.13	3.14 0.12	2.90 0.12	2.87 0.12
67B	0.280 0.071	11.83 0.48	7.51 0.27	7.40 0.17	7.30 0.13
166C	0.155 0.026	12.77 0.06	8.49 0.07	7.87 0.07	7.58 0.07
234A	0.179 0.047	12.78 0.04	8.49 0.06	7.92 0.04	7.65 0.04
234B	0.083 0.023	16.11 0.29	10.28 0.25	9.55 0.10	9.15 0.09
340A	0.657 0.101	—	4.73 0.12	4.23 0.12	4.25 0.12
340B	0.590 0.090	—	5.08 0.12	4.65 0.12	4.33 0.12
352A	0.195 0.060	10.80 0.20	7.13 0.19	6.59 0.19	6.38 0.19
352B	0.203 0.062	11.20 0.18	7.46 0.19	6.85 0.19	6.61 0.19
508A	0.709 0.179	8.43 0.17	5.72 0.17	5.12 0.17	4.95 0.17
508B	0.497 0.126	10.14 0.19	6.80 0.18	6.10 0.17	5.87 0.17
559A	1.086 0.025	4.71 0.05	3.24 0.05	3.00 0.05	2.90 0.05
559B	0.903 0.021	6.08 0.05	4.37 0.05	3.89 0.05	3.78 0.05
570B	0.553 0.047	9.39 0.09	6.24 0.08	5.66 0.09	5.47 0.08
570C	0.390 0.032	11.23 0.13	7.54 0.09	6.85 0.12	6.59 0.10
623A	0.511 0.182	11.11 0.10	7.32 0.07	6.83 0.07	6.58 0.07
623B	0.114 0.042	16.61 0.72	10.60 0.29	9.48 0.08	9.45 0.15
661A	0.264 0.020	10.82 0.08	7.14 0.05	6.60 0.05	6.40 0.06
661B	0.260 0.019	11.45 0.09	7.55 0.05	7.06 0.05	6.82 0.07
677A	0.285 0.092	8.37 0.22	5.65 0.21	5.10 0.21	4.94 0.22
677B	0.251 0.081	8.93 0.22	5.95 0.21	5.41 0.21	5.22 0.22
702A	0.856 0.056	5.70 0.06	4.15 0.06	—	3.90 0.05
702B	0.678 0.045	7.49 0.06	5.66 0.07	—	4.64 0.05
704A	0.932 0.187	3.95 0.15	2.62 0.16	2.47 0.15	2.38 0.17
704B	0.616 0.124	7.31 0.15	5.15 0.16	4.87 0.16	4.44 0.18
725A	0.370 0.061	11.18 0.05	7.48 0.03	6.95 0.03	6.72 0.03
725B	0.316 0.052	11.96 0.05	8.00 0.03	7.48 0.03	7.25 0.03
1245A	0.128 0.021	15.37 0.10	9.79 0.03	9.32 0.03	8.96 0.03
1245C	0.074 0.013	18.55 0.05	11.05 0.04	10.40 0.04	9.99 0.04
860A	0.257 0.011	11.81 0.07	7.88 0.04	7.30 0.04	6.99 0.04
860B	0.167 0.007	13.83 0.19	9.07 0.08	8.44 0.05	8.36 0.07

the Heintz orbit, and the substellar masses derived from that orbit are presumably in error. Observations during the approaching periastron passage should allow accurate mass determinations to be made within the next five years.

GL 644AB (Weis 1982; Heintz 1984; Pettersen *et al.* 1984): This pair, otherwise known as Wolf 630, is in fact a triple. Weis reported that the *B* component was twice as massive as *A*, and the total system mass found by Heintz also indicates a third body. A discussion of the radial velocity data on this complex system, which also includes VB 8 (GL 644C) and GL 643, is given by Pettersen. Speckle observations indicate that the two resolved components differ by 0.5 to 0.6 mag at near-infrared wavelengths.

GL 748AB (Lippincott 1977): With a period of ~2.5 yr, Wolf 1062 has a very low amplitude, but convincing, photocentric orbit semimajor axis of 0.026″. Thus, this star is difficult to resolve, given the estimated separation of ~0.1″. Speckle observations indicate that the companion is stellar, but we await better data before making an accurate mass determination.

GL 831AB (Lippincott 1979; McNamara *et al.* 1987): Otherwise known as the very close pair Wolf 922, this system is difficult because the components have never been observed separated by more than 0.25″. Both published orbits have periods under two years, but two infrared speckle observations, and the visible speckle point by Blazit *et al.* (1987) do not match the predicted position angles well for either orbit, and the mass sum from the formal derivation through Kepler's law results in a system mass $> 1.0 \mathcal{M}_\odot$, which appears unrealistic from the spectral type, fluxes and colors. The components differ by 1.2 to 1.9 mag in the infrared, allowing photometric estimates of the component masses to be made: $\sim 0.2 \mathcal{M}_\odot$ for the primary, and $\sim 0.1 \mathcal{M}_\odot$ for the secondary. Nearly all the error is in the determination of the semimajor axis, so further speckle work will yield accurate masses.

GL 866AB (McCarthy *et al.* 1987; Leinert *et al.* 1990): At a distance of only 3.4 parsecs, the components appear to be overmassive although the parallax appears well determined. No fractional mass is available for the pair because no astrometric orbit is available, thereby preventing the usual derivation of *B* as discussed in Sec. *3.1.1.* Until a fractional mass can be derived without invoking a mass–luminosity relationship, it is, of course, inappropriate to include these two points in the current MLRs.

3.2 Luminosities

3.2.1 Infrared magnitudes

The absolute infrared magnitudes for the components have been determined using the infrared photometry of the systems (Table 2), deconvolution of the photometry using the speckle observations (Table 2), and the parallaxes (Table 1). Table 5 lists the final infrared absolute magnitudes for the stars used in the MLRs.

Several sources of error have been considered in the calculation of the individual absolute magnitudes. The errors in the apparent photometry are as quoted in the reference, but were never taken to be less than 0.03 mag. This is in order to allow for possible flaring activity in the infrared (a topic which is currently unexplored), and for minor differences in photometric systems. Most of the photometry is from the compilation of Leggett (1992) who has carefully transformed all photometry to the CIT system for *J*, *H*, and *K*. For those binaries with photometry by this group on a similar, but not identical system, no conversion to the CIT system has been made, because errors in the absolute magnitudes are dominated by the formal errors in the speckle-determined magnitude differences and errors in

the parallaxes, both of which have been included in the final error calculation.

3.2.2 Visible magnitudes

Also listed in Table 5 are the absolute visual magnitudes, which cannot be measured directly in most cases. Optical speckle techniques are currently ineffective at measuring accurate brightness ratios for faint, close binaries, and instead we make use of the infrared–visible photometric relations discussed in Sec. *3.1.1* to estimate the M_V values. Only those stars with absolute infrared magnitudes falling within the limits of the calibrated relations have M_V listed, thus yielding 33 visual/speckle points for the MLR at V. The errors on M_V for the wide binaries include errors in the parallax and in the photometry—taken to be 0.05 mag, the mean error adopted by Leggett (1992). For the close binaries, the errors have been estimated using the range in the three M_V estimates from (1a), (1b), and (1c), combined in quadrature with errors due to uncertainties in the parallax.

In order to constrain the high mass end of the MLR at V, 38 stars with $\mathcal{M} \leqslant 2.00 \mathcal{M}_\odot$ have been taken from the work of Andersen (1991) on eclipsing binaries. Components of two systems, HD 6980 and HD 20301, have not been used because at least one, and possibly both components are evolved. In addition, the low-mass eclipsing binary system CM Dra has been added using the data in Popper (1980). Although the M_V values of the eclipsing binary components are not all on the same system, the errors are probably large enough (always $\geqslant$0.07 mag) to dominate any systematic errors. Unfortunately, because all of the systems are very close binaries, none could be resolved in the infrared on the 2.3 m telescope using speckle imaging.

4. RESULTS

4.1 The Mass–Luminosity Relations

The four panels of Fig. 2 show the empirical M_K, M_H, M_J, and M_V vs mass relations. The sizes of the points relate to the accuracy of the masses, corresponding to mass errors of 0%–10% (the largest points), 10%–20%, 20%–30%, and 30%–40%. The 38 stars in eclipsing binaries from Andersen (1991) and the two components of CM Dra from Popper (1980) are shown as open circles in the visual MLR, and have mass errors less than 10%. For the 36 eclipsing binary stars with masses 2.0 to $0.8 \mathcal{M}_\odot$, the mean errors are $0.02 \mathcal{M}_\odot$ in mass and 0.11 mag in M_V, much smaller than the points themselves. Components in the nearby visual and speckle binaries are shown as solid points with 1σ errorbars. Also shown are 1σ errors for stars in the two low mass eclipsing systems YY Gem and CM Dra.

Fits of many types, including linear, polynomial and spline fits, were attempted on the full datasets, and various portions. While some complicated fits for the entire datasets resulted in reasonable matches, simpler fits proved superior when the data were split into three sections, with divisions at 0.50 and $0.18 \mathcal{M}_\odot$. These limits have been chosen as boundaries of the obvious structure seen in all the plots near $\log \mathcal{M} = -0.5$. Moreover, by splitting the sample into sections, the structures of the MLRs at high masses do not drive the fits at low masses, and vice versa.

Linear fits weighted in the mass coordinate were made to the high mass [1.00 to $0.50 \mathcal{M}_\odot$] and low-mass [0.18 to $0.08 \mathcal{M}_\odot$] sections of each of the infrared MLRs, and are shown in panels (a), (b), and (c) of Fig. 2 with solid lines. Actual endpoints of the data used in the fits were 1.086 and $0.497 \mathcal{M}_\odot$ for the high mass region, and 0.179 and $0.074 \mathcal{M}_\odot$ for the low mass regime.

Between 0.50 and $0.18 \mathcal{M}_\odot$, the data are difficult to model—nearly all of the points in that region have similar absolute fluxes. This transition region is a result of the effects of H_2 opacity, coupled with the deepening convective region for lower mass stars (Kroupa *et al.* 1990). The net result is that as the mass decreases (and the temperature drops), more H_2 is formed, and while the luminosity continues to decrease, it does not drop per unit mass as quickly as it does in the high- and low-mass regions of the fit. Given the accuracy to which masses are currently known for stars 0.5 to $0.18 \mathcal{M}_\odot$, and in an effort not to overinterpret the data, we have adopted a tentative second-order fit through this region at all wavelengths, and have shown it with a dotted line. It is likely that there is another transition region corresponding to the stellar/substellar border near $0.08 \mathcal{M}_\odot$, below which there is only one object with an accurately determined mass, GJ 1245C. Further discussion of this second transition region can be found in Sec. *5.2*.

The three-part fits at infrared wavelengths are

$$\log(\mathcal{M}/\mathcal{M}_\odot) = -0.1048 M_K + 0.3217 \quad \text{(2a)}$$

for $1.00 \geqslant M \geqslant 0.50 \mathcal{M}_\odot$,

$M_K = 3.07$ to 5.94

rms in $\log(\mathcal{M}/\mathcal{M}_\odot) = 0.065$,

$$\log(\mathcal{M}/\mathcal{M}_\odot) = -0.2521 M_K + 1.1965 \quad \text{(2b)}$$

for $0.50 \geqslant M \geqslant 0.18 \mathcal{M}_\odot$,

$M_K = 5.94$ to 7.70

rms in $\log(\mathcal{M}/\mathcal{M}_\odot) = 0.089$

(0.238 with 352 and 677),

$$\log(\mathcal{M}/\mathcal{M}_\odot) = -0.1668 M_K + 0.5395 \quad \text{(2c)}$$

for $0.18 \geqslant M \geqslant 0.08 \mathcal{M}_\odot$,

$M_K = 7.70$ to 9.81

rms in $\log(\mathcal{M}/\mathcal{M}_\odot) = 0.067$,

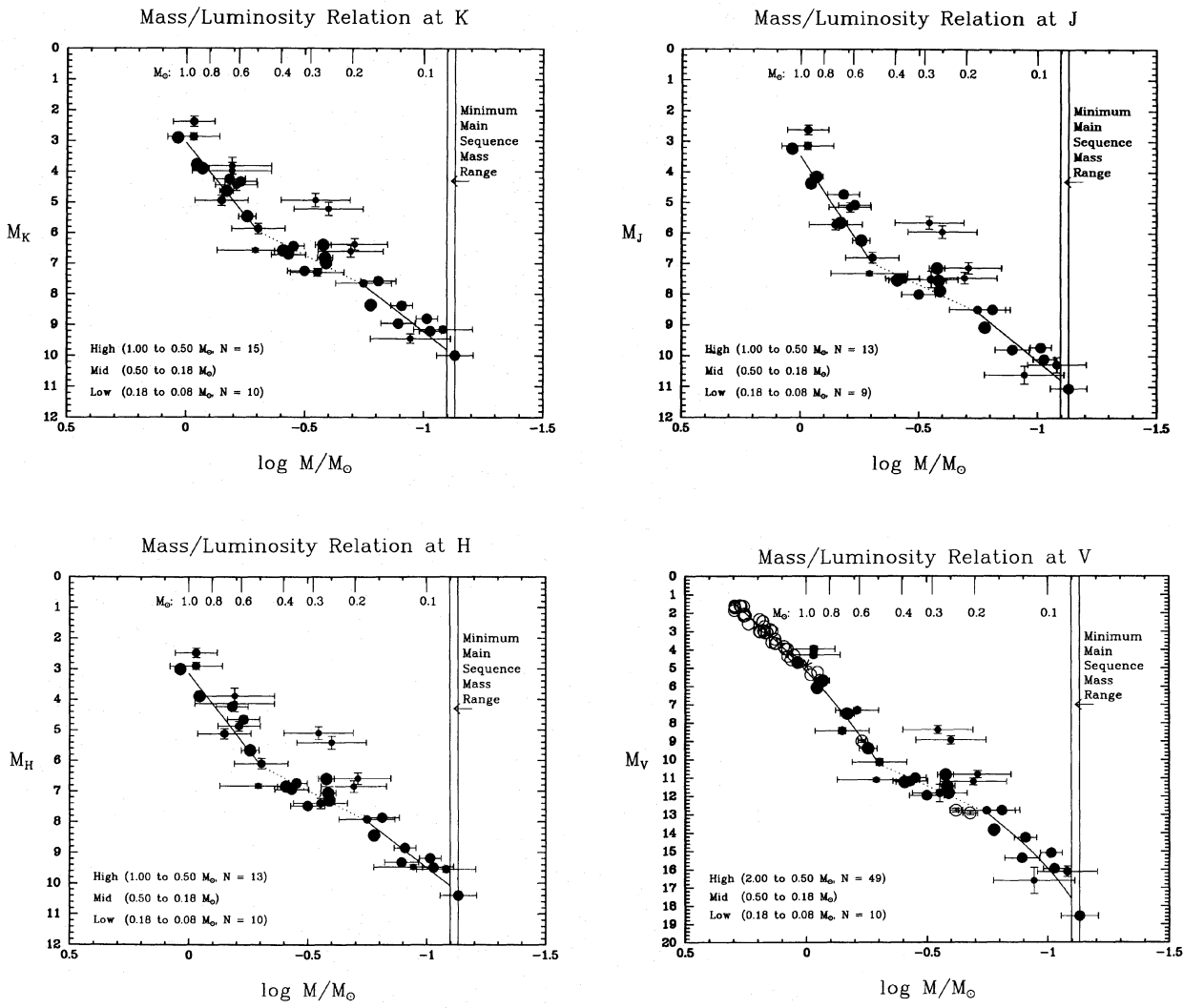

FIG. 2. The mass–luminosity relations at M_K, M_H, M_J, and M_V. The minimum main-sequence mass range adopted, 0.074 to 0.080$\mathcal{M}_\odot$, is shown with vertical lines. Fits to the three mass ranges discussed in the text are shown with solid and dotted lines. The section endpoints are given in the lower left of each panel, as well as the number of points used in the high and low mass range fits. The sizes of the points relate to the errors in the masses. In the M_V relation, the open points represent components in eclipsing binaries, and the asterisk represents the Sun.

$$\log q(\mathcal{M}/\mathcal{M}_\odot) = -0.1002 M_H + 0.3162 \quad (3a)$$

for $1.00 \geqslant M \geqslant 0.50 \mathcal{M}_\odot$,

$M_H = 3.15$ to 6.16

rms in $\log(\mathcal{M}/\mathcal{M}_\odot) = 0.067$,

$$\log(\mathcal{M}/\mathcal{M}_\odot) = -0.2451 M_H + 1.2090 \quad (3b)$$

for $0.50 \geqslant M \geqslant 0.18 \mathcal{M}_\odot$,

$M_H = 6.16$ to 7.97

rms in $\log(\mathcal{M}/\mathcal{M}_\odot) = 0.086$

(0.240 with 352 and 677),

$$\log(\mathcal{M}/\mathcal{M}_\odot) = -0.1675 M_H + 0.5906 \quad (3c)$$

for $0.18 \geqslant M \geqslant 0.08 \mathcal{M}_\odot$,

$M_H = 7.97$ to 10.08

rms in $\log(\mathcal{M}/\mathcal{M}_\odot) = 0.054$,

$$\log(\mathcal{M}/\mathcal{M}_\odot) = -0.0863 M_J + 0.3007 \quad (4a)$$

for $1.00 \geqslant M \geqslant 0.50 \mathcal{M}_\odot$,

$M_J = 3.48$ to 6.97

rms in $\log(\mathcal{M}/\mathcal{M}_\odot) = 0.055$,

$$\log(\mathcal{M}/\mathcal{M}_\odot) = -0.2791 M_J + 1.6440 \quad (4b)$$

for $0.50 \geqslant M \geqslant 0.18 \mathcal{M}_\odot$,

$M_J = 6.97$ to 8.56

rms in $\log(\mathcal{M}/\mathcal{M}_\odot) = 0.113$

(0.302 with 352 and 677),

$$\log(\mathcal{M}/\mathcal{M}_\odot) = -0.1592 M_J + 0.6177 \quad (4c)$$

for $0.18 \geqslant M \geqslant 0.08 \mathcal{M}_\odot$,

$M_J = 8.56$ to 10.77

rms in $\log(\mathcal{M}/\mathcal{M}_\odot) = 0.066$.

These relations can be applied to stars of mass 1.0 to 0.08 $\mathcal{M}_\odot$ in the appropriate sections, and supercede the fits reported in Henry & McCarthy (1990). Those relations had 29, 17, and 14 data points, whereas we now present 37, 35, and 33 points at *K*, *H*, and *J*, respectively. The structure in the MLR between 0.50 and 0.18 $\mathcal{M}_\odot$ is now evident, but could not be supported by the limited data available in 1990.

Two binaries are noticeably deviant from the MLR fits, GL 352AB and 677AB. Both systems have mass errors greater than 30% due to poorly determined parallaxes. Furthermore, GL 677AB is the most distant binary in the sample, and GL 352AB has only six reported observations. We anticipate that better parallaxes will bring the points into line. Regardless, both systems fall in the 0.50 and 0.18 $\mathcal{M}_\odot$ region, through which the ends of the high and low mass fits have simply been connected. Thus, these four points do not affect the "fit" shown by the dotted line in any way.

The rms value in $\log(\mathcal{M}/\mathcal{M}_\odot)$ for each portion of the MLRs is listed so that given an absolute magnitude, a mass can be estimated for an individual star (see Sec. *4.2 Warning* below for important caveats.) For example, given an $M_K = 9.00$, we find from the low-mass relation at *K* (2c) a mass of $0.109 \mathcal{M}_\odot$. The error on this value can be estimated using the rms of 0.067 in $\log(\mathcal{M}/\mathcal{M}_\odot)$. We find upper and lower values of 0.127 and 0.094 $\mathcal{M}_\odot$, yielding $\pm 0.017 \mathcal{M}_\odot$ as half of this range of values (error 16%). Similarly, an $M_K = 7.00$ star yields $0.270 \pm 0.056 \mathcal{M}_\odot$ (21% error) using (2b) and the rms value which does not include the GL 352AB and 677AB points. For $M_K = 5.00$, in the upper mass regime (2a), we determine a mass of $0.628 \pm 0.095 \mathcal{M}_\odot$ (15% error).

At visible wavelengths, third-order polynomial fits have been used in the high-mass and low-mass regions, because of the large number of points at high masses, and the apparent plummet in flux at very low masses (notably, the estimated M_V of GJ 1245C). The corresponding relations are

$$\log(\mathcal{M}/\mathcal{M}_\odot) = +0.002456 M_V^2 - 0.09711 M_V + 0.4365 \quad (5a)$$

for $2.00 \geqslant M \geqslant 0.50 \mathcal{M}_\odot$,

$M_V = 1.45$ to 10.25

rms in $\log(\mathcal{M}/\mathcal{M}_\odot) = 0.032$,

$$\log(\mathcal{M}/\mathcal{M}_\odot) = -0.1681 M_V + 1.4217 \quad (5b)$$

for $0.50 \geqslant M \geqslant 0.18 \mathcal{M}_\odot$,

$M_V = 10.25$ to 12.89

rms in $\log(\mathcal{M}/\mathcal{M}_\odot) = 0.081$

(0.257 with 352 and 677),

$$\log(\mathcal{M}/\mathcal{M}_\odot) = +0.005257 M_V^2 - 0.2351 M_V + 1.4124 \quad (5c)$$

for $0.18 \geqslant M \geqslant 0.08 \mathcal{M}_\odot$,

$M_V = 12.89$ to 17.59

rms in $\log(\mathcal{M}/\mathcal{M}_\odot) = 0.060$.

Tests of the accuracy of mass estimates in the three MLR ranges at *V* yield $0.099 \pm 0.014 \mathcal{M}_\odot$ (14% error) for $M_V = 16.00$, $0.254 \pm 0.048 \mathcal{M}_\odot$ (19% error, again using the rms without the GL 352AB and 677AB points) for $M_V = 12.00$, and $0.875 \pm 0.065 \mathcal{M}_\odot$ (7% error) for $M_V = 6.00$. Note the sizable error of the middle mass range estimate caused by the difficulty in modeling the data, and the accuracy of the upper mass range estimate, where the high quality eclipsing binary masses are used. This final error estimate exemplifies the cosmic scatter due to metallicity and age effects.

The sun [plotted in Fig. 2(d) with an asterisk] has not been used in developing these relations, due to the very different nature in which its mass and absolute magnitude must be determined. However, it provides an additional check on the strengths and limitations of the relations. At $M_V = 4.85$, (5a) yields a mass of $1.055 \mathcal{M}_\odot$, while the M_V relation would predict $M_V = 5.17$ at $1.000 \mathcal{M}_\odot$. Again, the differences in mass (6%) and M_V (0.3 mag) from the actual values are indicative of the cosmic scatter for the sample of stars in the high mass portion of the MLR. Ideally, given further information about age and metallicity for a stellar system, masses can be determined more accurately.

Finally, it is unlikely that many, if any, of the binary systems used in the infrared MLRs are unresolved triples. All are well-studied systems, and additional stellar components would probably have been detected during astrometric work, usually via an unusually high or low fractional mass. Of the 19 systems, four are known to have wide third components, and our speckle data indicates a possible close tertiary in only one case, GL 508AB.

4.2 Warning

A few caveats are in order when using any of these relations. First, we point out that the stars included in the

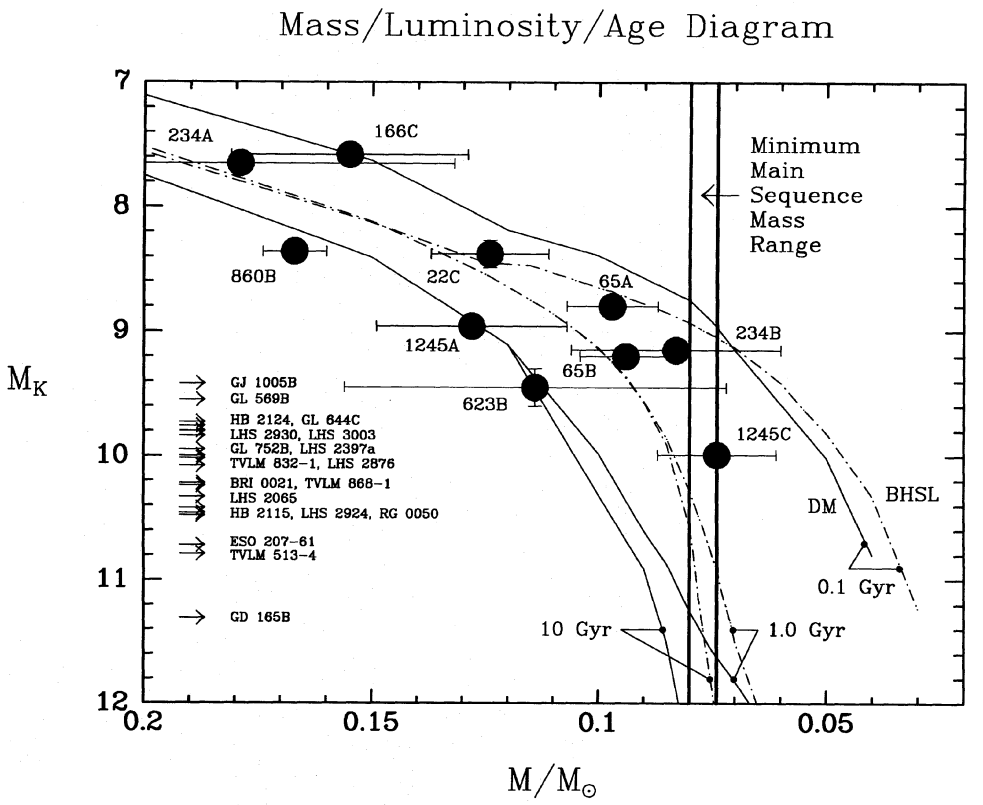

FIG. 3. The mass–luminosity–age diagram at M_K. Isochrones from the theoretical low-mass dwarf models of Burrows *et al.* (BHSL model H, 1992, dot–dash curves) and D'Antona & Mazzitelli (DM, 1985, solid curves) are shown for objects with ages 0.1, 1.0, and 10 Gyr. Shown at the left are very red dwarfs at their respective M_K values (see Table 6).

sample are of intermediate disk age, so the relations can only be applied accurately to objects of similar age. Of the nine systems included in Leggett's (1992) work, none appear to be halo objects, with a slight bias toward old disk ages, rather than young disk. In an effort to remove nearby binaries of exteme age from the sample, the subdwarf GL 53AB (McCarthy *et al.* 1992), the young, active system GL 566AB (Barry 1988), and the Hyades binary ADS3475 (Heintz 1986a) have *not* been included in the determination of the MLRs. Second, effects of metallicity have not been considered, as the limited sample size for subsets of stars within small mass ranges does not permit a detailed analysis. Andersen (1991) discusses the effects of evolution and metallicity upon stellar mass and luminosity determinations for stars with $\mathcal{M} \geqslant 1.0\mathcal{M}_\odot$. Third, the application of these relations to objects with masses less than $0.12\mathcal{M}_\odot$ ($M_K \sim 8.8$), where the theoretical models predict a growing spread in luminosities with age (see Sec. *5.1* and Fig. 3), must be done with suitable qualifications if no age estimate is available.

5. DISCUSSION

5.1 The Mass–Luminosity–Age Diagram

In addition to mass, age has a significant effect upon the flux emitted by a very low-mass star or brown dwarf, as illustrated in the mass–luminosity–age diagram (Fig. 3). Total luminosities for objects of masses 0.20 to $0.03\mathcal{M}_\odot$ at ages of 0.1, 1.0, and 10 Gyr have been taken from the D'Antona & Mazzitelli (1985, solid curves) and Burrows *et al.* (1989, 1992, dot–dash curves) evolutionary models for low-mass stars and brown dwarfs. The conversion from total luminosity to M_K has been accomplished using the very tight (correlation coefficient >0.99) empirical bolometric to K magnitude relation of Veeder (1974), which includes 96 objects with $4.0 \leqslant M_K \leqslant 9.5$:

$$M_{\rm bol} = 1.12 \cdot M_K + 1.81. \qquad (6)$$

We note that fainter than $M_K = 9.5$, where the relation is uncalibrated, the conversion from $L/L_\odot$ to M_K remains uncertain, so the curves shown in Fig. 3 at magnitudes fainter than 9.5 can only be regarded as guidelines. Note the precipitous drop in flux for a small change in mass across the stellar/substellar transition region. This is undoubtedly the reason why brown dwarfs of disk age, even when nearby, are so difficult to find.

The ten reddest objects with well determined masses are plotted using the information detailed in Table 5. All have had their infrared fluxes measured during the speckle work, and six rely upon speckle measurements for mass determination. In general, the agreement between observation and theory is relatively good, although for masses

TABLE 6. Low luminosity dwarfs.

Name	$\pi\pm\sigma$	Ref	M_K	M_V	(V−K)	(J−K)	Spec	Refs
GD 165 B	.0278 .0034	ZB	11.31	—	—	1.66	M10+	BZ,–,KHL
TVLM 513-4	.1008 .0023	TMR	10.79	—	—	1.19	—	TMR,–,–
ESO 207-61	.0504 .0026	I	10.72	18.90	8.18	1.19	—	RTR,RTR,–
RG 0050-2722	.0394 .0040	I	10.48	—	—	1.18	M8	RG,–,KHL
LHS 2924	.0908 .0013	M+	10.46	19.37	8.91	1.17	M9	L,L,KHM
HB 2115-4518	.0410 .0036	I	10.42	—	—	1.15	—	HB,–,–
LHS 2065	.1173 .0015	M+	10.33	19.15	8.82	1.26	M9	L,L,KHM
TVLM 868-1	.0575 .0019	TMR	10.24	—	—	1.28	—	TMR,–,–
BRI 0021-0214	.0825 .0034	TMR	10.22	—	—	1.26	—	TMR,–,–
LHS 2876	.0397 .0039	GJ	10.08	18.13	8.05	1.08	M6.5[b]	Bes,Bes,Bes
TVLM 832-1	.0394 .0022	TMR	10.02	—	—	1.12	—	TMR,–,–
LHS 2397a	.0700 .0021	M+	10.00	18.80	8.80	1.18	M8	L,L,KHL
GJ 1245 C	.2206 .0021	Har	9.99[a]	18.55[a]	8.56[a]	1.06[a]	—	*,*,–
GL 752 B	.1701 .0008	M+	9.95	18.65	8.70	1.10	M8	L,L,KHM
LHS 3003	.1524 .0035	I	9.84	17.96	8.12	1.00	M6.5[b]	L,L,Bes
LHS 2930	.1038 .0014	M+	9.80	17.96	8.16	0.97	M6.5	L,L,Boe
GL 644 C	.1545 .0007	M+	9.76	17.74	7.98	0.95	M7	L,L,KHM
HB 2124-4228	.0324 .0057	I	9.73	—	—	1.22	—	HB,–,–
GL 569 B	.0956 .0114	GJ	9.55	—	—	1.13	M8.5	BZ,–,HK
GL 623 B	.1317 .0039	GJ	9.45[a]	16.61[a]	7.16[a]	1.15[a]	—	*,*,–
GJ 1005 B	.1887 .0084	GJ	9.42[a]	16.72[a]	7.30[a]	1.01[a]	—	*,*,–
GL 234 B	.2421 .0017	GJ	9.15[a]	16.11[a]	6.96[a]	1.13[a]	—	*,*,–
0.074 $M_\odot$			10.0	18.3	8.3	1.0		this work
0.080 $M_\odot$			9.8	17.6	7.8	1.0		this work

Notes to TABLE 6

[a] indicates value derived from infrared speckle data and relations in this paper

[b] spectral type on Bessel system (1991), all other types on Kirkpatrick *et al.* system (1991)

References for TABLE 6

BZ = Becklin & Zuckerman (1988),
Bes = Bessell (1991),
Boe = Boeshaar (1992),
GJ = Gliese and Jahreiss (1991),
Har = Harrington (1990),
HB = Hawkins & Bessell (1988),
HK = Henry & Kirkpatrick (1990),
I = Ianna (1992, 1993),
KHL = Kirkpatrick *et al.* (1993),
KHM = Kirkpatrick *et al.* (1991),
L = Leggett (1992),
M+ = Monet *et al.* (1992),
RG = Reid & Gilmore (1981),
RTR = Ruiz *et al.* (1991),
TMR = Tinney *et al.* (1993),
ZB = Zuckerman & Becklin (1992),
* = this work

$<0.12\mathcal{M}_\odot$, the models indicate that as a group, the objects are relatively young, with ages 0.1 to 1.0 Gyr. However, using the space motions of the four systems represented, the velocity diffusion coefficient method of Wielen (1977) leads to age estimates of 7 Gyr for GL 65, 5 Gyr for GL 623, 3 Gyr for GL 234 and 1 Gyr for GJ 1245, indicating that this small subsample is not preferentially young. Alternately, Leggett (1992) has found that the GL 65 system belongs to the young disk population, GL 234 to the young or old disk, and GL 623 to the old disk or halo population. GJ 1245 was not classified. These estimates, in fact, are consistent with the trend in Fig. 3—GL 623 appears to be the oldest of the three. However, these examples are so few that further discussion must be deferred until more objects are known and accurate masses are available.

Nonetheless, in the case of the D'Antona and Mazzitelli models, all but one of the points, Kruger 60B, fall within the age boundaries shown. A new model from the more sophisticated work by Burrows *et al.* has been kindly provided by Didier Saumon. This model, known as H in their latest paper (Burrows *et al.* 1992), does not include all of their latest improvements, but is representative of the stars in the solar neighborhood, with $Y_\alpha=0.28$, $Z=Z_\odot$, and the mixing length parameter set equal to unity. Again, the match of their models to the data is good, given the errors

on the masses, except for the Kruger 60B point.

5.2 Guidelines for the End of the Main Sequence

Keeping in mind the qualifications discussed in Sec. *4.2*, it is instructive to estimate empirical guidelines marking the edges of the stellar/substellar transition region. Here we compute absolute magnitudes and colors for 0.074 and 0.080 $\mathcal{M}_\odot$ (roughly 70 and 75 Jupiter masses) using the empirical MLRs. While we have chosen these values to define the transition region between stars and brown dwarfs, we emphasize that this range is a function of the helium fraction, metallicity and mixing length used in the models. The two chosen values, illustrated with vertical stripes in Figs. 2 and 3, represent the range of Burrows *et al.* (1992) terminal points for the main sequence assuming helium fractions of 0.22 to 0.28, solar metallicity, and a mixing length of unity. For $Z=0$, their models indicate a main sequence terminus as high as 0.098 $\mathcal{M}_\odot$.

From (2c), (3c), (4c), and (5c), we find the following absolute magnitudes and colors for the edges of the transition region:

$$0.074\mathcal{M}_\odot\text{: } M_K\sim 10.0,\ M_H\sim 10.3,\ M_J\sim 11.0,\ M_V\sim 18.3,$$

$$(V-K)\sim 8.3,\ (J-K)\sim 1.0$$

$$0.080\mathcal{M}_\odot\text{: } M_K\sim 9.8,\ M_H\sim 10.1,\ M_J\sim 10.8,\ M_V\sim 17.6,$$

$$(V-K)\sim 7.8,\ (J-K)\sim 1.0.$$

We stress that these values are for illustrative purposes only. It is not appropriate to assign a particular value to the end of the main sequence, and it would be incorrect to do so because the MLR for these very low-mass objects is a strong function of age and composition. Nonetheless, these values indicate that several objects already known in the solar neighborhood have characteristics indicative of objects with masses lying in or below the transition region for some ages. Of course, we will only be certain that an object is a true brown dwarf when its mass is determined to be well below 0.08 $\mathcal{M}_\odot$.

On the left of Fig. 3 we illustrate the members of a growing collection of very low luminosity red dwarfs, including several brown dwarf candidates. To the best of our knowledge, the list of red dwarfs in Table 6 includes all those known with $M_K>9.7$, requiring, of course, that the trigonometric parallax is known and that K photometry is available. Absolute K and V magnitudes, colors, and spectral types are given, and the final column gives three references for the infrared photometry, V photometry, and spectral type, respectively. Unfortunately, in most cases, the masses remain undetermined because they are single objects, or in wide, slow-orbiting, binaries. Also included in the table are the four very low-mass dwarfs found in the solar neighborhood, GJ 1245C, GL 623B, GJ 1005B, and GL 234B, which have ranges of possible masses straddling the transition region, and the brown dwarf candidate GL 569B. Phil Ianna has kindly provided several provisional parallaxes, including that of ESO 207-61. Of all the objects listed, the standout is GD 165B, at present the best brown dwarf candidate.

6. FUTURE

The foundation of the mass–luminosity relation through the lower main sequence has been established using the combination of long-term astrometric studies and infrared speckle imaging. Of the ten lowest luminosity objects with well determined masses, nine were included in our completed northern M dwarf survey to eight parsecs, and the tenth, GL 22C at 10 pc, was discovered by this group (McCarthy *et al.* 1991). Thus, infrared speckle work provides the cornerstone around which the description of the lowest mass stars is being built—of the 35 masses $\leqslant 0.5\mathcal{M}_\odot$ known for red dwarfs (including 10 with preliminary mass estimates in binaries that are the subjects of continuing speckle work), 19 depend upon infrared speckle imaging data, and nine were first imaged using the technique.

In Sec. *3.1.4*, several systems were discussed that will be the targets of future speckle work, and which will allow further refinement of the very low mass portion ($\leqslant 0.18\mathcal{M}_\odot$) of the MLRs. The infrared MLRs could obviously be extended to higher masses through studies of eclipsing binaries at infrared wavelengths.

Now that an accurate mass–luminosity relation has been determined for stars of low mass, a luminosity function for the nearby M dwarfs will yield an accurate mass function, which is arguably the best way to describe the stellar population. This is one topic to be discussed in a future paper, in which we will report the results of our completed infrared speckle search for low mass companions orbiting nearby M dwarfs (Henry & McCarthy 1990, 1992). With an accurate mass function in hand, we will then be able to find the contribution of red dwarfs to the galactic mass in the solar neighborhood. In this paper we have calibrated the mass–luminosity relation for the most populous members of the galaxy, including those objects near the stellar/substellar border, and we are now poised to address these larger questions concerning the Sun's nearest neighbors.

We would like to thank Jonathan Freeman and Julian Christou for their valuable assistance in the development and use of the speckle data reduction software. We are especially indebted to Phil Ianna, Didier Saumon, and Scott Kenyon for allowing us to use recent, unpublished data. Finally, we express our gratitude to the referee, whose thorough critique has led to a much-improved paper. This work has been supported by National Science Foundation Grants Nos. AST 88-22465 and AST 92-03336. T.J.H. wishes to acknowledge current support from the NASA High Resolution Microwave Survey.

REFERENCES

Andersen, J. 1991, A&Ar, 3, 91
Baize, P. 1955, J. Observateurs, 38, 42
Barry, D. C. 1988, ApJ, 334, 436
Becklin, E. E., & Zuckerman, B. 1988, Nature, 336, 656
Bessell, M. S. 1991, AJ, 101, 662
Blazit, A., Bonneau, D., & Foy, R. 1987, A&AS, 71, 57
Boeshaar, P. 1992, private communication
Burrows, A., Hubbard, W. B., & Lunine, J. I. 1989, ApJ, 345, 939
Burrows, A., Hubbard, W. B., Saumon, D., & Lunine, J. I. 1992, ApJ (submitted)
D'Antona, F., & Mazzitelli, I. 1985, ApJ, 296, 502
Demarque, P., Guenther, D. B., & van Altena, W. F. 1986, ApJ, 300, 773
Eggen, O. J. 1967, ARA&A, 5, 105
Elias, J. H., Frogel, J. A., Matthews, K., & Neugebauer, G. 1982, AJ, 87, 1029
Engels, D., Sherwood, W. A., Wamsteker, W., & Schultz, G. V. 1981, A&AS, 45, 5
Feierman, B. H. 1971, AJ, 76, 73
Geyer, D. W., Harrington, R. S., & Worley, C. E. 1988, AJ, 95, 1841
Gliese, W., & Jahreiss, H. 1991, Preliminary Version of the Third Catalog of Nearby Stars
Harmanec, P. 1988, Bull. Astron. Inst. Czechosl., 39, 329
Harrington, R. S. 1990, AJ, 100, 559
Hawkins, M. R. S., & Bessell, M. S. 1988, MNRAS, 234, 177
Heintz, W. D. 1969, AJ, 74, 768
Heintz, W. D. 1972, AJ, 77, 160
Heintz, W. D. 1974, AJ, 79, 819
Heintz, W. D. 1976, ApJ, 208, 474
Heintz, W. D. 1979, AJ, 84, 1223
Heintz, W. D. 1982, Observatory, 102, 42
Heintz, W. D. 1984, PASP, 96, 439
Heintz, W. D. 1986a, AJ, 92, 446
Heintz, W. D. 1986b, A&AS, 65, 411
Heintz, W. D. 1987, PASP, 99, 1084
Heintz, W. D. 1989, A&A, 217, 145
Heintz, W. D. 1990, Observatory, 110, 131
Heintz, W. D., & Borgman, E. R. 1984, AJ, 89, 1068
Henry, T. J., Johnson, D. S., McCarthy, Jr., D. W., & Kirkpatrick, J. D. 1992, A&A, 254, 116
Henry, T. J., & Kirkpatrick, J. D. 1990, ApJ, 354, L29
Henry, T. J., & McCarthy, Jr., D. W. 1990, ApJ, 350, 334
Henry, T. J., & McCarthy, Jr., D. W. 1992, in Complementary Approaches to Double and Multiple Star Research, edited by H. A. McAlister and W. I. Hartkopf (Astronomical Society of the Pacific, San Francisco), p. 10
Henry, T. J., McCarthy, Jr., D. W., Freeman, J., & Christou, J. C. 1992, AJ, 103, 1369
Hershey, J. L. 1973, AJ, 78, 935
Hershey, J. L. 1982, AJ, 87, 145
Ianna, P. A. 1993, in CCD Parallaxes for Southern Very Low Luminosity Stars, IAU Symposium No. 156, P. 75
Ianna, P. A. 1993, private communication
Ianna, P. A., Rohde, J. R., & McCarthy, Jr., D. W. 1988, AJ, 95, 1226
Johnson, D. S., Henry, T. J., & McCarthy, Jr., D. W. 1993, in preparation
Johnson, H. L., MacArthur, J. W., & Mitchell, R. I. 1968, ApJ, 152, 465
Kamper, K. W., & Wesselink, A. J. 1978, AJ, 83, 1653
Kenyon, S. J. 1993, private communication
Kirkpatrick, J. D., Henry, T. J., & Liebert, J. 1993, ApJ, 406, 701
Kirkpatrick, J. D., Henry, T. J., & McCarthy, Jr., D. W. 1991, ApJS, 77, 417
Kroupa, P., Tout, C. A., & Gilmore, G. 1990, MNRAS, 244, 76
Leggett, S. K. 1992, ApJS, 82, 351
Leinert, C., Haas, M., Allard, F., Wehrse, R., McCarthy, Jr., D. W., Jahreiss, H., & Perrier, C. 1990, A&A 236, 399
Liebert, J., & Probst, R. G. 1987, ARA&A, 25, 473
Lippincott, S. L. 1977, AJ, 82, 925
Lippincott, S. L. 1979, PASP, 91, 784
Lippincott, S. L. 1982, AJ, 87, 1237
Lippincott, S. L., & Borgman, E. R. 1978, PASP, 90, 226
Lippincott, S. L., Braun, D., & McCarthy, Jr., D. W. 1983, PASP, 95, 271
Marcy, G. W., & Benitz, K. J. 1989, ApJ, 344, 441
Marcy, G. W., & Moore, D. 1989, ApJ, 341, 961
Mariotti, J.-M., Perrier, C., Duquennoy, A., & Duhoux, P. 1990, A&A 230, 77
McAlister, H. A. & Hartkopf, W. I. 1988, Second Catalog of Interferometric Measurements of Binary Stars, CHARA Contribution No. 2
McCarthy, Jr., D. W. 1986, in Astrophysics of Brown Dwarfs, edited by M. C. Kafatos, R. S. Harrington, and S. P. Maran (Cambridge University Press, Cambridge), p. 9
McCarthy, Jr., D. W., Cobb, M. L., & Probst, R. G. 1987, AJ, 93, 1535
McCarthy, Jr., D. W., *et al.* 1993, AJ, 105, 652
McCarthy, Jr., D. W., & Henry, T. J. 1987, ApJ, 319, L93
McCarthy, Jr., D. W., Henry, T. J., Fleming, T. A., Saffer, R. A., Liebert, J., & Christou, J. C. 1988, ApJ, 333, 943
McCarthy, Jr., D. W., Henry, T. J., McLeod, B. A., & Christou, J. C. 1991, AJ, 101, 214
McCarthy, Jr., D. W., McLeod, B. A., & Barlow, D. 1990, Proc. SPIE, 1237, 496
McNamara, B. R., Ianna, P. A., & Fredrick, L. W. 1987, AJ, 93, 1245
Monet, D. G., Dahn, C. C., Vrba, F. J., Harris, H. C., Pier, J. R. Luginbuhl, C. B., & Ables, H. D. 1992, AJ, 103, 638
Morbey, C. L., & Griffin, R. F. 1987, ApJ, 317, 343
Pettersen, B. R., Evans, D. S., & Coleman, L. A. 1984, ApJ, 282, 214
Popper, D. M. 1980, ARA&A, 18, 115
Probst, R. G. 1977, AJ, 82, 656
Probst, R. G. 1981, Ph.D. thesis, University of Virginia
Probst, R. G., & Liebert, J. 1983, ApJ, 274, 245
Rakos, K. D. *et al.* 1982, A&AS, 47, 221
Reid, I. N., & Gilmore, G. 1981, MNRAS, 196, 15P
Ruiz, M. T., Takamiya, M. Y., & Roth, M. 1991, ApJ, 367, L59
Smith, R. C. 1983, Observatory, 103, 29
Stauffer, J. R., & Hartmann, L. W. 1986, ApJS, 61, 531
Strand, K. A. 1963, in Basic Astronomical Data, edited by D. L. Harris III, K. A. Strand, and C. E. Worley (University of Chicago Press, Chicago), p. 282.
Tinney, C. G., Mould, J. R., & Reid, I. N. 1993, AJ, 105, 1169
Tokovinin, A. A. 1992, A&A, 256, 121
van den Bos, W. H. 1937, Union Obs. Circ., 4, 342
van den Bos, W. H. 1938, Union Obs. Circ., 4, 448
Veeder, G. J. 1974, AJ, 79, 1056
Weilen, R. 1977, A&A, 60, 263
Weis, E. W. 1982, AJ, 87, 152
Worley, C. E., & Heintz, W. D. 1983, Fourth Catalog of Orbits of Visual Binary Stars, Pub. of the USNO, Vol. 24, part 7
Worth, M. D., & Heintz, W. D. 1974, ApJ, 193, 647
Zuckerman, B., & Becklin, E. E. 1992, ApJ, 386, 260